RESCEU No.24/95

X-Ray Properties of the Nucleus of M81

Yoshitaka Ishisaki, Kazuo Makishima, and Naoko Iyomoto
Department of Physics, School of Science, University of Tokyo, Hongo, Bunkyo-ku, Tokyo 113
E-mail (YI) ishisaki@miranda.phys.s.u-tokyo.ac.jp
Kiyoshi Hayashida
Department of Earth and Space Science, Osaka University, Machikaneyama, Toyonaka, Osaka 560
Hajime Inoue, Kazuhisa Mitsuda, Yasuo Tanaka, and Shin'ichiro Uno
Institute of Space and Astronautical Science, 3-3-1 Yoshinodai, Sagamihara, Kanagawa 229
Yoshiki Kohmura
Institute for Physical and Chemical Research, 2-1 Hirosawa, Wako, Saitama 351-01
Richard F. Mushotzky, Robert Petre, and Peter J. Serlemitsos
Laboratory for High Energy Physics, NASA/GSFC, Greenbelt, MD 20771, USA
and
Yuichi Terashima
Department of Astrophysics, Nagoya University, Chikusa-ku, Nagoya 464-01

PASJ: Publ. Astron. Soc. Japan **48**, 1–9 (1996)

X-Ray Properties of the Nucleus of M81

Yoshitaka ISHISAKI, Kazuo MAKISHIMA, and Naoko IYOMOTO
Department of Physics, School of Science, University of Tokyo, Hongo, Bunkyo-ku, Tokyo 113
E-mail (YI) ishisaki@miranda.phys.s.u-tokyo.ac.jp
Kiyoshi HAYASHIDA
Department of Earth and Space Science, Osaka University, Machikaneyama, Toyonaka, Osaka 560
Hajime INOUE, Kazuhisa MITSUDA, Yasuo TANAKA, and Shin'ichiro UNO
Institute of Space and Astronautical Science, 3-3-1 Yoshinodai, Sagamihara, Kanagawa 229
Yoshiki KOHMURA
Institute for Physical and Chemical Research, 2-1 Hirosawa, Wako, Saitama 351-01
Richard F. MUSHOTZKY, Robert PETRE, and Peter J. SERLEMITSOS
Laboratory for High Energy Physics, NASA/GSFC, Greenbelt, MD 20771, USA
and
Yuichi TERASHIMA
Department of Astrophysics, Nagoya University, Chikusa-ku, Nagoya 464-01

(Received 1995 September 25; accepted 1996 January 30; to appear in the Publ. Astron. Soc. Japan **48**, 1996)

Abstract

Due to the appearance of SN 1993J, the region of M81 (NGC 3031) was observed with ASCA ten times between 1993 April and 1995 April. Data from the eight of these observations are used to study the 0.5–10 keV spectral and temporal properties of the source designated X-5, coincident with the M81 nucleus. The 2–10 keV luminosity of X-5 varied by a factor of 1.7 in two years, around a mean of $\sim 2 \times 10^{40}$ erg s^{-1}. Variations by $\sim$ 20 % on a time scale of one day were also detected. The average spectrum of X-5 can be represented in the 2–10 keV range by a power-law continuum of photon index $\Gamma = 1.85 \pm 0.04$ and a relatively low intrinsic absorption column of $N_{\rm H} \sim 1 \times 10^{21}$ cm^{-2}. In the soft ($<$ 2 keV) energy range, an additional thermal component with a temperature 0.6–0.8 keV is detected. An apparently broad or complex Fe-K emission line centered at 6.6–6.7 keV was also detected at an equivalent width of 170 ± 60 eV. These results indicate that the M81 nucleus is a low luminosity active galactic nucleus, and suggest that similar objects are relatively numerous. A comparison is made between the nucleus of M81 and those of Seyfert galaxies.

Key words: Galaxies: active — Galaxies: individual (M81) — Galaxies: X-rays

1. Introduction

M81 (NGC 3031) is a nearby (D $\sim$ 3.6 Mpc; Freedman et al. 1994) early-type spiral galaxy with a prominent bulge and well defined spiral arms. Its nucleus shows weak Seyfert-like activity in the optical (Peimbert, Torres-Peimbert 1981; Shuder, Osterbrock 1982; Filippenko, Sargent 1988; Ho et al. 1995, 1996) and radio (Bartel et al. 1982; Beck et al. 1985) frequencies, and is considered to host a low-ionization nuclear emission-line region (LINER; e.g. Filippenko, Sargent 1985).

There are several different physical mechanisms that can give rise to the LINER phenomenon, including enhanced starburst activity (e.g. Terlevich, Melnick 1985) and the presence of an active galactic nucleus (AGN; which we identify with an accreting massive black hole) of low luminosity (e.g. Kwan, Krolik 1981). Although optical information is sometimes inadequate to distinguish between these two alternatives, in the X-ray band there is clear spectral difference between them. Starburst galaxies have thermal X-ray spectra with emission lines from ionized metals (Makishima 1994, hereafter MA94; Tsuru et al. 1994; Serlemitsos et al. 1995b, hereafter SEA95), while AGNs exhibit power-law X-ray continua of photon index $\Gamma \sim 1.7$ (e.g. Turner, Pounds 1989) and often fluorescent Fe-K lines (e.g. Pounds et al. 1990; Awaki et al. 1991; Nandra 1991). X-ray variability (e.g. Krolik et al. 1993) provides more evidence for the presence of an AGN.

M81 has been observed in X-rays with Einstein (Elvis, van Speybroeck 1982; Fabbiano 1988, hereafter FA88), EXOSAT (Barr et al. 1985), Ginga (Ohashi et al. 1992; Tsuru 1992), BBXRT (Petre et al. 1993; hereafter PEA93), and ROSAT (Boller et al. 1992). The Ein-

stein data (FA88) revealed the presence of several X-ray sources in the M81 region, among which the brightest one, called X-5, coincides in position with the M81 nucleus and has an angular size $< 4''$ (< 70 pc; Elvis, van Speybroeck 1982). In these previous observations, X-5 exhibited a 2–10 keV luminosity a few times 10^{40} erg s^{-1}, together with evidence of long-term variability and an episode of rapid flux change (Barr et al. 1985). These X-ray studies have led to the conclusion that X-5 is a low-luminosity AGN (LLAGN) in M81. However, discrepant spectra have been obtained for X-5 with Einstein ($\Gamma = 4^{+2}_{-1.5}$) and other observations ($\Gamma = 2.0$–2.2; Boller et al. 1992; Ohashi et al. 1992; Tsuru 1992; PEA93).

Due to the explosion of SN 1993J in M81 on 1993 March 28 (Garcia 1993), just 5 weeks after the launch of ASCA (Tanaka et al. 1994), we have frequently observed the M81 region with ASCA. Results on SN 1993J from these observations have been reported by Kohmura et al. (1994) and Kohmura (1994). These observations have also provided data of unprecedented quality and quantity on M81 X-5, which was always in the same ASCA field of view as SN 1993J. These results greatly strengthen the case that X-5 is an LLAGN. Some of these ASCA results on X-5 have already been reported by Ishisaki (1994) and SEA95.

2. Observations and Data Reduction

2.1. Observations

We observed the M81 region ten times with ASCA, as summarized in table 1. Six of these were performed between April 5 and May 19 in 1993 during the performance verification (PV) phase, almost once a week. The subsequent four observations were performed at intervals of six months as dictated by sun-angle constraints of the satellite (Tanaka et al. 1994).

In these observations, data from the two GIS (Gas Imaging Spectrometer; Kohmura et al. 1993; Ohashi et al. 1996) detectors, GIS2 and GIS3, were always taken in the PH normal mode. For the observations 1 through 6, the GIS spread discriminator was disabled, which caused a high background toward the detector rims, and a faint spill-over of counts from the ^{55}Fe calibration isotope at certain positions on the detector plane (which does not affect the present results). The observation modes of the two SIS (Solid-State Imaging Spectrometer; Burke et al. 1991, 1994) detectors, SIS0 and SIS1, are listed in table 1. Each SIS detector comprises four CCD chips named C0 through C3.

2.2. X-ray images

In figure 1 we show examples of the SIS and GIS images of the M81 region. There were thus always three X-ray sources in the SIS field of view (figure 1a): X-5 at the M81 nucleus, the Einstein source X-6 (probably a bright X-ray binary; FA88), and SN 1993J. The 0.5–10 keV raw intensities of X-5 and X-6 were in the range 0.32–0.56 and 0.05–0.07 c s^{-1} per each SIS detector, respectively (Kohmura 1994). The 0.5–10 keV SIS intensity of SN 1993J was ~ 0.08 c s^{-1} (per SIS) in the first two observations, and then declined with a typical e-folding time of ~ 70 days (Kohmura 1994). Thus, by the time when the ASCA images in figure 1 were obtained, SN 1993J had become much fainter (~ 0.02 c s^{-1} or less) than in early observations (Kohmura et al. 1994).

In the GIS image (figure 1b), SN 1993J and X-6 are confused because their angular separation ($\sim 1'$) is smaller than the GIS position resolution. In addition to X-5, X-6 and SN 1993J, we always detected another Einstein source, X-9, which is probably a background quasar (FA88). The GIS data for X-9 indicate a flat power-law ($\Gamma \sim 1.7$) spectrum and a moderate (factor ~ 1.5) intensity variation. These results on X-9, as well as on X-6, will be reported in a forthcoming paper (Uno et al. 1996, in preparation), in which the latest results on SN 1993J will also be described.

2.3. Data reduction

In the present paper, we utilize both the SIS and GIS data. For the SIS, we use only the faint mode data to avoid a subtle (typically by 10–30 eV) energy-scale ambiguity due to offset in the zero point (known as Dark Frame Error; Otani, Dotani 1994). We discard the SIS and GIS data from the first two observations, because, on these occasions, SN 1993J was too bright (subsection 2.2) to ignore its contamination of X-5, and the SIS data were taken entirely in bright mode.

For the SIS event selection from the remaining eight observations, we require the geomagnetic cut-off rigidity to be > 6 GeV c^{-1}, and the elevation angle from the night and day earth rim to be $> 10°$ and $> 25°$, respectively. For the GIS event selection, we use the same cut-off rigidity and a minimum earth elevation angle $> 5°$. These criteria have left us with 343 ks of good data for the GIS and 175 ks for the SIS.

The point spread function of the ASCA X-ray telescope (XRT; Serlemitsos et al. 1995a; Tsusaka et al. 1995) caused significant contamination within the X-5 region from SN 1993J and X-6, which are $2.'8$ and $3.'4$ away from X-5, respectively. If we adopt $1.'5$ (or $3.'0$) as the integration radius around X-5, roughly 30 % (or 70 %) of the photons from SN 1993J and 30 % (or 50 %) of the photons from X-6 falls onto the X-5 accumulation region. Further taking into account the relative intensities among the three sources (subsection 2.2), we have set the integration radius around X-5 to be $1.'5$ for observations 3 and 4 when SN 1993J was bright, and $3.'0$ for the subsequent observations to collect as many signal photons

as possible. The contribution from SN 1993J plus X-6 to the events accumulated around X-5 is estimated to be 5–10 % at most.

For the spectral analysis and flux calculations, we subtract the background (the cosmic X-ray background plus non X-ray background; Kubo et al. 1994; Ikebe et al. 1995; Makishima et al. 1996) accumulated over the same detector positions using blank-sky data (the M81 galaxy background is not subtracted, and estimated later in subsection 3.4.). For the SIS, the publicly released data (Gendreau 1994) were used. We made the GIS background from the Lynx field and the Lockman Hole data for observations 1–6 when the spread discriminator was still off, while we used the NEP, QSF3, Draco and SA57 fields for observations 7–10 which occurred after the spread discriminator was enabled.

The XRT+SIS and XRT+GIS response files have been calculated separately for the four detectors, and separately for each observation, because on different occasions the target was observed at different positions in the field of view. The responses take into account all the known instrumental characteristics of the XRT (Kunieda et al. 1995; Tsusaka et al. 1995), the SIS (Burke et al. 1991, 1994), and the GIS (Ishida et al. 1994; Makishima et al. 1996).

3. Results

3.1. Intensity and spectrum variability

In figure 2a we present the background-subtracted long-term light curve of X-5 in the 2–10 keV band, for observations 5–10. The flux has been calculated using the instrumental responses mentioned above. We have omitted the results from observations 3 and 4, due to the relatively large flux uncertainties associated with the small integration radius required because of SN 1993J. Thus, the four detectors consistently indicate that the X-5 flux varied significantly over $(1.4\text{–}2.4) \times 10^{-11}$ erg cm^{-2} s^{-1}, by a factor ~ 1.7, implying a 2–10 keV luminosity range of $(2.1\text{–}3.5) \times 10^{40}$ erg s^{-1} (employing the 3.6 Mpc distance). We estimate these absolute flux levels to be reliable within $\sim \pm 15$ %.

Figure 3 shows the short-term light curve of X-5 from observation 9. Both instruments thus suggest an overall ~ 20 % intensity decline, particularly toward the latter half of the observation, which is far too large to be caused by spacecraft attitude jittering. When the light curves are examined against the hypothesis of constant intensity, we obtain $\chi^2/\nu = 217/68$ with the SIS and 183/88 with the GIS, so that the hypothesis is rejected. We therefore conclude that a short-term intensity change was detected in this particular observation, on a time scale of about a day. A similar short-term variation was seen in observation 3, as reported by SEA95. There is no evidence for such short-term variation in the other observations, with typical upper limits of ~ 15 %. We recall that a rapid (~ 600 s) variation was once recorded from M81 by EXOSAT (Barr et al. 1985), and possibly with the Einstein IPC (FA88).

The X-5 spectra are relatively featureless. In order to get a rough idea of spectral variation, we fitted the 2–10 keV spectra from individual observations, separately for the two instruments, with a power-law model. We used the instrumental responses derived in subsection 2.3. The fit evaluation includes 3 % systematic errors. An acceptable fit was obtained in all cases. As shown in figure 2b, the spectral variability is statistically insignificant, in spite of the clear long-term intensity variation. We estimate the spectral index to have remained constant within ± 0.05, around the mean value of $\Gamma \sim 1.81$.

3.2. Average 2–10 keV spectra

Since the spectral variations are insignificant, we summed up all the SIS (SIS0+SIS1) data into a single spectrum, and all the GIS (GIS2+GIS3) data into another, as shown in figure 4. Unlike in the previous subsection, we have included the data from observations 3 and 4 as well. This has allowed us to utilize one of the longest exposure times (343 ks for the GIS and 175 ks for the SIS) achieved with ASCA for a single object. We also calculated average XRT+SIS and XRT+GIS responses, as averages of those for individual observations (subsection 2.3) weighted by the number of detected signal photons. Using these responses, we fitted the summed SIS and GIS spectra separately in the 2–10 keV range with thermal bremsstrahlung and power-law models. As shown in table 2, the bremsstrahlung model could fit neither spectrum well ($\chi^2/\nu \sim 3.5$). This confirms the BBXRT result (PEA93), but with much higher significance.

The power-law model with $\Gamma \sim 1.8$ was much more successful (table 2), indicating that the 2–10 keV continuum from X-5 definitely prefers a non-thermal interpretation to a thermal one. The obtained values of $\Gamma \sim 1.8$ are consistent with those derived from individual observations (figure 2b). However, these fits were still unacceptable, because of significant positive residuals in the 6–7 keV range in both spectra (figure 4). This feature was not significant in the individual spectra because of insufficient statistics. The feature is most naturally attributed to Fe-K emission lines, which have been observed mainly at 6.4 keV (corresponding to ionization states less than Fe XVIII) from a number of AGNs (e.g. Pounds 1990; Awaki et al. 1991; Nandra 1991). However, in the present case, the line appears broader than the instrumental energy resolutions (~ 0.1 and ~ 0.45 keV for the SIS and the GIS respectively, in FWHM).

In order to model the line feature, we fitted the summed 2–10 keV spectra with a power-law model, plus a Gaussian of which the center, width, and normalization were left free. The fit is improved, especially for the GIS spectrum (table 2), as far as the Gaussian is allowed to be broad. Therefore, the presence of the line feature and its intrinsic width are both statistically significant. However, as shown in figure 5, the line parameters from the two instruments can be reconciled only at the 99 % confidence level, and the SIS fit remains unacceptable (which makes the SIS contours in figure 5 rather meaningless). Since the SIS response exhibits more complex long-term changes (Otani, Dotani 1995) than the GIS, we suspect that our particular SIS spectrum, averaged over many observations spanning 2 years, may be subject to larger systematic errors. In fact, using a subset of the present ASCA data on X-5, SEA95 derived Fe-K line parameters from the two instruments that are both consistent with the present GIS results. We therefore refer mainly to the GIS-derived Fe parameters in the following, and defer detailed comparison of the SIS and GIS Fe line parameters to a forthcoming paper (Yaqoob et al. 1996, in preparation).

Are the iron line photons really coming from the X-5 region? In fact, a broad Fe-K line centered at ~ 6.8 keV was detected from SN 1993J (Kohmura et al. 1994; Kohmura 1994). However the calculated contamination from SN 1993J can explain at most 15 % of the line photons seen in the X-5 spectra. Furthermore the iron line source is mostly confined within $\sim 3'$ (~ 3 kpc) of the M81 nucleus, since the line flux did not increase significantly when we increase the data integration radius around X-5 up to $6'$. We thus conclude that almost all the observed iron line photons are coming from the data integration region around X-5.

In Seyfert galaxies, a spectral hump is produced in the 7–20 keV range by Compton-reflection effects (Pounds et al. 1990; Awaki et al. 1991). In search of this effect in the X-5 data, we added a strongly absorbed power-law component to fit the average GIS spectrum. We tied its photon index to that of the main power-law, and fixed its absorption to 3×10^{23} cm^{-2} to approximate the reflection effect (Awaki et al. 1991). However, even allowing the main power-law and Gaussian parameters to float, the reflection component was not required, with its normalization < 12 % (90 % confidence) of the main power-law. This is significantly lower than is typically found (~ 30 %) in Seyfert galaxies (Pounds et al. 1990).

3.3. Spectra in the full energy range

In order to fully utilize the spectroscopic capabilities of ASCA, we expanded the range of the power-law plus Gaussian fit to 0.5–10 keV for the SIS, and 0.7–10 keV for the GIS. We allowed both Γ and the column density $N_{\rm H}$ to float. For fitting the SIS (or GIS) spectrum, we fixed the Gaussian parameters at those obtained above 2 keV with the SIS (or GIS). Results of these fits are summarized in table 3. Although the value of Γ is similar to those obtained in 2–10 keV, the fit is not acceptable for either spectrum because of slight data excess in the < 2 keV range.

We accordingly added a Raymond-Smith (R-S) plasma emission component (Raymond, Smith 1977) to the model spectrum, as is often seen in the spectra of spiral galaxies (MA94; SEA95). We left its temperature and normalization free, and assumed that it is absorbed only by the Galactic line-of-sight column. We fixed the R-S abundance at 0.4 times solar (MA94; SEA95), assuming the solar abundance ratios. Then, as shown in table 3, the GIS fit has become acceptable, indicating that the soft component is statistically significant. The R-S temperature, 0.6–1.1 keV, is similar to those obtained in other spirals (see subsection 4.6); Γ remained nearly unaffected by introducing the soft component. The best-fit models are shown in figure 6 together with the full-range spectra. However, the thermal flux required by the SIS spectrum is much less than that required by the GIS spectrum, and the SIS and GIS values for the column density to the power-law component are inconsistent with each other. Furthermore, the SIS fit is still formally unacceptable. These problems did not vanish even if we let the overall abundance float.

The above discrepancy could arise if the thermal emission is extended, because the poorer position resolution of the GIS would then reduce the contrast of the nuclear point source relative to the extended emission. To examine this possibility, we again varied the data integration radius, but the fit parameters did not change significantly for either instrument. This means that the thermal source is mostly confined within $3'$ (3 kpc) of the nucleus, as for the Fe-K line. Resolving the remaining spectral discrepancy between the two instruments would require further effort of instrumental calibration, which is beyond the scope of the present paper.

3.4. Background emission from the M81 galaxy

Our data integration radii around X-5 are relatively large (1.6 kps or 3.1 kpc). Therefore, before ascribing the X-5 properties to the M81 nucleus, we must evaluate possible contamination from "galaxy background", i.e., various non-nuclear X-ray components in M81. Although the soft R-S component may prevail below ~ 2 keV, above 2 keV the largest contribution is expected to come from low-mass X-ray binaries (LMXBs; Fabbiano 1989). The brightest LMXBs have been resolved with Einstein (Elvis, van Speybroeck 1982; FA88), while fainter ones will make an unresolved extended background (FA88). The Einstein sources X-2, X-3, and X-7 (FA88) fall in

the larger of our two integration radii, while X-6 and SN 1993J make partial contributions (subsection 2.3).

We derived a 2–10 keV radial X-ray brightness profile around X-5, by integrating the GIS data from observations 7–9, over a position angle range $-135°$ to $45°$ (to avoid X-6, SN 1993J, and X-9). Its comparison with the point spread function has revealed an extended emission outside $\sim 3'$, up to at least $10'$. This galaxy background shows a 2–10 keV luminosity of $\sim 2 \times 10^{39}$ erg s^{-1} when integrated over the $180°$ sector of $3' - 10'$ annulus, and its 0.7–10 keV spectrum can be fitted well with a moderately absorbed ($< 3 \times 10^{21}$ cm^{-2}), hot (> 8 keV) bremsstrahlung. Comparing these results with those from M31 (Makishima et al. 1989), we can safely ascribe the observed M81 galaxy background to the integrated emission from LMXBs. However within $\sim 3'$ of the nucleus, the galaxy background brightness is highly uncertain, because the X-5 radial profile becomes indistinguishable from the point spread function.

To more directly evaluate the LMXB contribution to the X-5 spectra of figure 4, we fitted them using a model consisting of a power-law, a Gaussian, and a LMXB component (a thermal Bremsstrahlung with temperature fixed to 10 keV, absorbed with a fixed column of 2×10^{21} cm^{-2}; Makishima et al. 1989). The SIS and GIS spectra consistently restricted the LMXB contribution to < 12 % (90 % confidence) of the 2–10 keV luminosity of X-5. This is consistent with the spill-over flux from X-6 and SN 1993J as estimated in subsection 2.3. Even allowing the largest possible LMXB contribution, Γ steepens only by 0.03. We thus conclude that the ASCA spectra of X-5 are approximately free from the galaxy background.

We also examined the ROSAT HRI image (figure 1b) taken from the archival data, where the nucleus, off-nuclear point sources including SN 1993J, and diffuse or unresolved galaxy emission are seen. The nucleus exhibited a similar luminosity (Boller et al. 1992) as we observed. We found that, of the total ~ 6200 HRI signal X-rays within $3'$ of the nucleus, at least 82 % is confined to within $0.'5$. The galaxy background within $3'$ is thus estimated to be 18 % at most in the soft X-ray band, and this must partially be coming from the soft thermal emission as we observed (figure 6). Therefore, the galaxy background within $3'$ must be even lower in > 2 keV, thus providing an independent support to the above conclusion.

4. Discussion

4.1. Identification of X-5 with the active nucleus of M81

We have detected a factor ~ 1.7 X-ray variation from X-5 over a time span of 2 years, and the observed 2–10 keV flux range is consistent with those recorded from past observations, $(1.4\text{–}2.9) \times 10^{-11}$ erg cm^{-2} s^{-1} (table 3 of PEA93). We also detected ~ 20 % intensity changes on time scales of a day. These results establish the variability of X-5 much more convincingly than before. This, combined with the clear non-thermal nature of the X-5 spectra above 2 keV (table 2), makes the starburst interpretation of X-5 unlikely.

The variability implies that X-5 consists of a single, or at most a small number of, presumably accretion-powered compact object(s). However, an assembly of ordinary LMXBs cannot provide an explanation, since X-5 is pointlike (< 70 pc; Elvis, van Speybroeck 1982), and the observed X-5 spectra are inconsistent with those of LMXBs. In addition, the 2–10 keV luminosity of X-5, $\sim 2 \times 10^{40}$ erg s^{-1} on the average, would require $\sim 10^2$ LMXBs emitting at the Eddington limit, so that the variability would be much smaller than was observed. Therefore as argued by Elvis, Van Speybroeck (1982), X-5 must either be an LLAGN, or a "super-Eddington" X-ray source as are sometimes found in nearby galaxies (Fabbiano 1989).

In spite of the excellent data quality, the ASCA spectra of X-5 above ~ 2 keV are well characterized by a single power-law (plus the iron line), with little contribution from the LMXB-type component. From tables 2 and 3, we quote the photon index to be $\Gamma = 1.85 \pm 0.04$. (In figure 2, Γ is somewhat smaller since the Fe-K line was not separately modeled.) This spectrum is similar to those of Seyfert nuclei, but not with the spectra of super-Eddington sources which generally resemble those of LMXBs (MA94; Okada et al. 1994). Considering further the positional coincidence of X-5 with the M81 nucleus (within $\sim 10''$; Elvis, Van Speybroeck 1982), we can confirm the identification of X-5 as an LLAGN made by previous X-ray observations and optical investigations (Filippenko, Sargent 1988; Ho et al. 1996).

4.2. Possible prevalence of LLAGNs

The M81 nucleus exhibits an Hα emission line with a broad component, and its Hα to X-ray luminosity ratio is similar to those of Seyfert galaxies (Elvis, Van Speybroeck 1982; Filippenko, Sargent 1988). We therefore infer that the optical lines from M81 are powered by the power-law X-rays from the LLAGN.

Besides M81, LLAGNs have so far been established in a fair number of nearby galaxies (MA94; SEA95), including, e.g., M106=NGC 4258 (Makishima et al. 1994; Miyoshi et al. 1995), NGC 3642, NGC 4278 (Koratkar et al. 1995), M104=NGC 4594 (Terashima et al. 1994), NGC 1097 (Iyomoto et al. 1996), and M51=NGC 5194 (Makishima et al. 1990; MA94; Terashima et al. 1996, in preparation). These galaxies are classified as LINERs, and furthermore, exhibit weak but broad Hα component. We therefore suggest that LINERs, particularly those with broad Hα components, have a rather high proba-

bility to harbor LLAGNs. Since LINERs are rather numerous (Filippenko, Sargent 1985; Ho et al. 1995), this further suggests that a fair fraction of apparently normal galaxies host LLAGNs.

The 2–10 keV luminosities of these LLAGNs, typically (1–10) $\times$ 10^{40} erg s^{-1}, smoothly connect to the lowest end of the Seyfert luminosity function ($10^{41.5-44}$ erg s^{-1}). Therefore, the AGN luminosity function may well extend below $\sim$ 10^{42} erg s^{-1} (Mushotzky 1993; Koratkar et al. 1995; SEA95), and the LLAGN contribution to the cosmic X-ray background may not be ignored. This inference supports the prediction by Elvis et al. (1984) based on the Hα luminosity distributions, but it may contradict the results by Persic et al. (1989).

4.3. Hard power-law continuum

The power-law index $\Gamma = 1.85 \pm 0.04$ we derived for the M81 nucleus is consistent with those of type 1 Seyferts (SEA95) as well as that of the M106 nucleus ($\Gamma = 1.78 \pm 0.29$; Makishima et al. 1994) which is another convincing example of LLAGN (Miyoshi et al. 1995). However, our value of Γ is significantly smaller (flatter) than those obtained for the M81 nucleus with previous X-ray studies. Even putting aside the very steep index of $\Gamma = 4^{+2}_{-1.5}$ (FA88) obtained with the Einstein IPC (which may be related to the marked faintness of X-5 at that time; see PEA93), observations with EXOSAT, Ginga, BBXRT, and ROSAT consistently yielded $\Gamma = 2.0 - 2.2$ with relatively small uncertainties (table 3 of PEA93). Time variability cannot provide a solution to this discrepancy, since during the ASCA observations Γ stayed in the range 1.7–1.9 while the X-ray flux was consistent with those observed previously except the Einstein IPC flux (PEA93).

Among these previous results, the EXOSAT ME (Barr et al. 1985) and the Ginga LAC (Ohashi et al. 1992) results were obtained with non-imaging proportional counters, so that they may be contaminated by other point sources (e.g. X-9; FA88) in the M81 region and by extended emission components associated with M81. The BBXRT spectrum may have been contaminated similarly, even though the soft thermal component was resolved spectrally by PEA93. On the other hand, the ROSAT PSPC result (Boller et al. 1992), although based on an image, may have been affected by the thermal emission from the nuclear region (which we detected), since the value of $\Gamma = 2.0^{+0.16}_{-0.15}$ was derived via a simple single-model fit. Thus, the steeper spectra obtained previously can be explained away in a reasonable way.

We have obtained a relatively small intrinsic absorption ($< 2 \times 10^{21}$ cm^{-2}) for the hard component of the M81 nucleus (a factor of 2–4 smaller than was obtained by PEA93). This makes a contrast to the case of the M106 nucleus which is absorbed with $\sim 1.5 \times 10^{23}$ cm^{-2} (Makishima et al. 1994). Considering that the M106 nucleus is certainly seen almost edge-on through the molecular disk (Miyoshi et al. 1995), the difference in absorption between the nuclei of M81 and M106 is most naturally attributed to the difference in the viewing angle with respect to the gaseous disk around the nucleus. This is essentially the same as unification models which account for the difference between type 1 and type 2 Seyfert galaxies (e.g. Antonucci, Miller 1985; Awaki et al. 1991).

These spectral properties make LLAGNs look in many respects like scaled-down versions of Seyfert galaxies. However the trend seen in Seyfert 1/2 galaxies, that the fraction of obscured objects increases with decreasing intrinsic luminosity (Lawrence, Elvis 1982), does not seem to extend to LLAGNs (Mushotzky 1993). The Compton reflection effect may be less significant in LLAGNs than in Seyfert galaxies (subsection 3.2; Mushotzky 1993). Furthermore there are two more X-ray dissimilarities between the M81 nucleus and Seyfert galaxies; Fe-K line energy, and rapid variability (Mushotzky 1993), which we discuss in the following two subsections. These suggest that caution should be exercised before regarding LLAGNs and Seyfert galaxies as a single and homogeneous class of objects.

4.4. Iron emission line

We have detected an iron-K emission line from the M81 nucleus with an equivalent width of $\sim$ 170 eV. Although PEA93 did not detect narrow Fe-K lines from the M81 nucleus with an upper limit equivalent width of 90 eV, their results may be reconciled with ours by the fact that we observed the line to be apparently broad (Gaussian $\sigma \sim 0.2$ keV; figure 5). Evidence of an Fe-K emission line centered at 6.77 ± 0.45 keV was obtained in the Ginga spectrum of M81 plus M82, and its equivalent width becomes 330 ± 210 eV if all the line photons are assumed to come from M81 (Tsuru 1992). Considering the absence of Fe-K lines in the ASCA spectrum of M82 (Tsuru et al. 1994), this may actually be the case, suggesting consistency between the Ginga and ASCA observations.

The Fe-K lines from AGNs are generally thought to arise via reprocessing of the hard power-law continuum from the nucleus by surrounding material (e.g. the accretion disk; e.g. Pounds et al. 1990; Awaki et al. 1991; Nandra 1991). When the reprocessing material is nearly neutral, we expect a fluorescence Fe-K line to appear at 6.40 keV in the local rest frame (Makishima 1986). When the material is significantly photoionized so that the dominant ionization states are helium-like or hydrogen-like, the Fe line will appear at rest-frame energies of 6.7 or 6.9 keV, respectively.

The iron line profile of the M81 nucleus is reminiscent of the broad and asymmetric Fe-K line profiles observed with ASCA from several Seyfert galaxies (Fabian et al.

1994; Mushotzky et al. 1995; Tanaka et al. 1995), which have been interpreted in terms of gravitational redshift and Doppler effects in the accretion disks seen with an inclination of $\sim 20^\circ$. However, while the iron line flux in these Seyfert galaxies is mostly limited to < 6.4 keV in the source rest frame, the present results indicate a considerably higher center energy, 6.65 ± 0.15 keV (figure 5). This is one difference between the M81 nucleus and AGN.

This difference in the line center energy may be explained in several ways (SEA95). First, the M81 line photons may be a blend of separate narrow lines: e.g., a 6.4 keV line and a 6.7 keV line. In fact, the GIS line feature can also be modeled by two narrow lines at ~ 6.3 and ~ 6.8 keV, although the SIS data somewhat prefer a single broad line. Second, it is possible that the accretion disk has a higher inclination than those in Seyfert 1 galaxies ($\sim 20^\circ$), so that blue-shifted component due to the longitudinal Doppler effect is enhanced. Indeed, in the type 2 Seyfert galaxy IRAS 18325-5926, a broad iron line has been observed at 6.8–6.9 keV in the source rest frame (Iwasawa et al. 1995). A third possibility is that the line-producing region in the M81 nucleus is significantly more photoionized than in those of Seyfert galaxies. Further discussion on the Fe-K line will be made in a forthcoming paper (Yaqoob et al. 1996, in preparation).

4.5. Time variation

Some Seyfert galaxies (particularly of low-luminosity ones) exhibit pronounced intensity variations on time scales as short as 10^{3-4} s, by more than a factor of a few (e.g. Lawrence et al. 1987; McHardy, Czerny 1987; Kunieda et al. 1992; Krolik et al. 1993). In contrast, variations of the M81 nucleus on these time scales were much less conspicuous; even on longer time scales, its variation (figure 2a) is considerably smaller than those of Seyfert galaxies. Filippenko, Sargent (1988) and Ho et al. (1996) report that the Hα emission from the M81 nucleus is stable, unlike in Seyfert galaxies. No rapid X-ray variability was detected from the LLAGNs in M106 (Makishima et al. 1994) or in NGC 1097 (Iyomoto et al. 1996), either. These pieces of evidence provide another potential difference between LLAGNs and Seyferts (Mushotzky et al. 1993)

The power-density spectrum (PDS) $P(\nu)$ of intensity variation in Seyfert galaxies and Galactic black-hole candidates can be modeled as

$$P(\nu) = \begin{cases} P_0 & (\nu < \nu_k) \\ P_0\,(\nu/\nu_k)^{-\alpha} & (\nu > \nu_k) \end{cases} \qquad (1)$$

where P_0, α, and ν_k (knee frequency) are constants. Seyfert galaxies typically exhibit $\alpha = 1$–2 (Lawrence et al. 1987; McHardy, Czerny 1987; Hayashida et al. 1995), and Hayashida et al. (1995) derived $\nu_k \sim 5 \times 10^{-5}$ Hz for NGC 4051 and MCG-6-30-15. From Galactic black-hole candidates, we typically observe $\alpha \sim 1.4$ and $\nu_k \sim 0.1$ Hz (e.g. Makishima 1989).

Suppose we repeatedly observe an X-ray source whose PDS is represented by eq. (1), determine the intensity over an integration time T_1 each, and obtain a light curve of a total time span T_2 ($T_1 << T_2$). Then, even for a fairly uneven data sampling, the root-mean-square fractional variation V of the light curve may be approximated as

$$V(T_1, T_2)^2 = c \int_{\nu_2}^{\nu_1} P(\nu)\, d\nu \qquad (2)$$

where $\nu_i = {T_i}^{-1}$ ($i = 1, 2$), and c is an appropriate constant. In the present case, the long-term light curve (figure 2) gives $T_1 = 3 \times 10^4$ s (typical duration of each observation; table 1) and $T_2 = 6 \times 10^7$ s (2 years) together with $V(T_1, T_2) = 0.22$, while the short-term light curve (figure 3) implies $T_1 = 600$ s, $T_2 = 2 \times 10^4$ s, and $V(T_1, T_2) = 0.08$. By substituting these results into eq. (2), and utilizing eq. (1) with $\alpha = 1.5$, we can eliminate the normalization product $P_0\, c$. We have thus obtained for the M81 nucleus $\nu_k = (1$–$3) \times 10^{-6}$ Hz. This knee frequency is significantly lower than those of the rapidly varying Seyferts, and seems closer to that of some quasars (Hayashida et al. 1995).

Although the physical mechanism accounting for eq. (1) is not understood, a lower value of ν_k is thought to indicate a longer scale length, hence a larger black-hole mass (e.g. Wandel, Mushotzky 1986; Hayashida et al. 1995). We therefore suggest that the mass of the M81 nucleus, and of other LLAGNs in general, is larger than those of the fast-varying Seyfert nuclei, and their very low luminosities are a result of extremely small accretion rates (Iyomoto et al. 1996). Actually, M106 has a nuclear mass of $3.6 \times 10^7\ M_\odot$ (Miyoshi et al. 1995) and an accretion rate as small as $\sim 7 \times 10^{-6}$ times the Eddington accretion rate (derived from the ASCA luminosity of Makishima et al. 1994). However we cannot yet exclude the possibility that the reduced variability in LLAGNs is a direct consequence of the very low accretion rate itself, rather than due to the large central mass. X-ray variation is insignificant also in some type 2 Seyfert galaxies (e.g. NGC 1068; Ueno et al. 1994), presumably due to the predominance of reprocessed X-ray components. However this cannot be the case in the M81 nucleus, since it lacks reprocessing signatures such as absorption edges, very flat X-ray continua ($\Gamma \sim 1.3$; Ueno et al. 1994), Compton reflection components (subsection 3.2), or *neutral* fluorescence lines (Fukazawa et al. 1994).

4.6. Soft thermal emission

Within 3 kpc of the M81 nucleus, we have detected thermal emission with a sub-keV temperature and a 0.5–3 keV luminosity of $(0.4$–$1.5) \times 10^{39}$ erg s^{-1}. If we assume

that the extended (or unresolved) X-ray emission seen in the ROSAT HRI map (subsection 3.4) has a similar thermal spectrum, its 0.5–3 keV luminosity in an annular region of radius $0.'5 - 3'$ from the nucleus is estimated to be $\sim 1 \times 10^{39}$ erg s^{-1}, which agrees with the ASCA results. On the other hand, PEA93 obtained evidence for a similar thermal component using BBXRT, but their thermal flux is 5–20 times larger than ours. Presumably as a result of the larger aperture, the BBXRT spectrum included a significant contribution from a much larger part of the M81 galaxy.

From a number of spiral galaxies, ASCA has detected similar soft thermal X-ray components which have typical temperatures of 0.5–1.0 keV and often sub-solar abundances (MA94; Terashima et al. 1994; SEA95; Iyomoto et al. 1996). The 0.5–4 keV luminosities of such components vary from galaxy to galaxy over the range 10^{38-40} erg s^{-1} (SEA95). These components may well come from heterogeneous origins, including supernova remnants, hot plasmas associated with jets (e.g. in M106; Makishima et al. 1994), thermal gas created in the nuclear starburst region (e.g. in M82; Tsuru et al. 1994), and reprocessing of the hard nuclear X-rays by photoionized material. Thus, the nature of the M81 thermal component is yet to be investigated.

5. Summary and Conclusion

Through a series of observations of the M81 region with ASCA, we have shown that its nucleus can be regarded as an LLAGN (low-luminosity AGN). We observed both long-term and short-term intensity variations. The characteristic time scale of variation of the M81 nucleus is inferred to be ~ 10 days, which may be longer than those of Seyfert galaxies but similar to those of quasars. We speculate that some LLAGNs, if not all, have larger central masses than Seyfert galaxies.

The spectrum of the M81 nucleus consists of a hard power-law continuum, an iron-K line, and a soft thermal component. The power-law index was found to be stable at $\Gamma \sim 1.85$, with relatively low intrinsic absorption ($\sim 1 \times 10^{21}$ cm^{-2}). Therefore the M81 nucleus can be regarded as a typical LLAGN without heavy obscuration, in contrast to the strongly absorbed M106 nucleus. The nature of the thermal component is yet to be specified.

The observed iron line is broad ($\sigma \sim 0.2$ keV), or complex, and exhibits an equivalent width of 170 ± 60 eV. When compared to the Fe-K lines observed from Seyfert galaxies, the Fe-K line of the M81 nucleus has a similar profile but a significantly higher line center energy (~ 6.65 keV). This difference allows several alternative explanations.

We thank all the members of the ASCA team for the mission management, including spacecraft operation, data acquisition, and instrumental calibration. We thank Tahir Yaqoob and Andy Ptak for helpful discussions and comments.

References

Antonucci R. R., Miller J. S. 1985, ApJ 297, 621
Awaki H., Koyama K., Inoue H., Halpern J. 1991, PASJ 43, 195
Barr P. et al. 1985, Bull Am Astr Soc 17, 608
Bartel N. et al. 1982, ApJ 262, 556
Beck R., Klein U., Krause M. 1985, A&A 152, 237
Boller Th., Meurs E. J. A., Brinkmann W., Fink H., Zimmermann U., Adorf H.-M. 1992, A&A 261, 57
Burke B. E., Mountain R. W., Daniels P. J., Dolat V. S. 1994, IEEE Trans. Nuc. SCI. 41, 375
Burke B. E., Mountain R. W., Harrison D. C., Bautz M. W., Doty J. P., Ricker G. R., Daniels J. P. 1991, IEEE Trans. ED-38, 1069
Elvis M., Soltan A., Keel W. C. 1984, ApJ 283, 479
Elvis M., Van Speybroeck L. 1982, ApJL 257, L51
Fabian A. C. et al. 1994, PASJ 46, L59
Fabbiano G. 1988, ApJ. 325, 544 (FA88)
Fabbiano G. 1989, ARAA 27, 87
Filippenko A. V., Sargent W. L. W. 1985, ApJS 57, 503
Filippenko A. V., Sargent W. L. W. 1988, ApJ 324, 134
Freedman W. L. et al. 1994, ApJ 427, 628
Fukazawa Y. et al. 1994, PASJ 46, L141
Garcia F. 1993, IAU Circ. No.5731
Gendreau K. C. 1994, ASCA Newsletter (NASA/GSFC) 2, 5
Hayashida K. et al. 1995, ApJ, submitted
Ho L. C., Filippenko A. V., Sargent W. L. W. 1995, ApJS 98, 477
Ho L. C., Filippenko A. V., Sargent W. L. W. 1996, ApJ in press (Feburuary 1 issue)
Ikebe Y., Ishisaki Y., Kubo H., Idesawa E., Takahashi T. Makishima K., the GIS team 1995, ASCA Newsletter (NASA/GSFC) 3, 13
Ishida M. et al. 1994, ASCA Newsletter (NASA/GSFC) 2, 20
Ishishaki Y. 1994, in New Horizon of X-Ray Astronomy, ed F. Makino, T. Ohashi (Universal Academy Press, Tokyo) p505
Iwasawa K. et al. 1995, MNRAS, submitted
Iyomoto N. et al. 1996, PASJ in press
Kohmura Y. 1994, PhD Thesis, University of Tokyo (Physics Department)
Kohmura Y. et al. 1993, Proc. SPIE 2006, 79
Kohmura Y. et al. 1994, PASJ 46, L157
Koratkar A., Deustua S. E., Heckman T., Filippenko A. V., Ho L. C., Rao M. 1995, ApJ 440, 132
Krolik J., Done C., Madejsli G. 1993, ApJ 402, 432
Kubo H., Ikebe Y., Makishima K., the GIS team 1994, ASCA Newsletter (NASA/GSFC) 2, 14
Kunieda H., Furuzawa A., Watanabe M., and the XRT team 1995, ASCA Newsletter (NASA/GSFC) 3, 3
Kunieda H., Hayakawa S., Tawara Y., Koyama K., Tsuruta S., Leighly K. 1992, ApJ 384, 482
Kwan J., Krolik J. 1981, ApJ 250, 478

Lawrence A., Elvis M. 1982, ApJ 256, 410
Lawrence A., Watson M., Pounds K., Elvis M. 1987, Nature 325, 694
Makishima K. 1986, in Physics of Accretion onto Compact Objects, ed K. O. Mason, M. G. Watson, N. E. White (Springer-Verlag, Berlin) p249
Makishima K. 1989, in Physics of Neutron Stars and Black Holes, ed Y. Tanaka (Universal Academy Press, Tokyo) p175
Makishima K. 1994, in New Horizon of X-Ray Astronomy, ed F. Makino, T. Ohashi (Universal Academy Press, Tokyo) p171 (MA94)
Makishima K. et al. 1989, PSJ 41, 697
Makishima K. et al. 1994, PASJ 46, L77
Makishima K. et al. 1996, PASJ, submitted
Makishima K., Ohashi T., Kondo, H., Palumbo G. G. C., Trinchieri G. 1990, ApJ 365, 159
McHardy I., Czarny B. 1987, Nature 325, 696
Miyoshi M., Moran J., Herstein J., Greenhill L., Nakai N., Diamond P., Inoue M. 1995, Nature 373, 127
Mushotzky R. F. 1993, in The Nearest Active Galaxies, ed J. Beckman, L. Colina, H. Netzer (Consejo Superior de Investigaciones Cientificicas Madrid) p47
Mushotzky R. F., Fabian A. V., Iwasaka K., Kunieda H., Matsuoka M, Nandra K., Tanaka Y. 1995, MNRAS 272, L9
Nandra K. 1991, PhD Thesis, Leicester University
Ohashi T. et al. 1992, in Windows on Galaxies, ed G. Fabbiano et al. (Kluwer Academic Press; Dordrecht) p243
Ohashi T. et al. 1996, PASJ, submitted
Okada K., Mihara T., Makishima K. 1994, in New Horizon of X-Ray Astronomy, ed F. Makino, T. Ohashi (Universal Academy Press, Tokyo) p515
Otani C., Dotani T. 1994, ASCA Newsletter (NASA/GSFC) 3, 25
Peimbert M., Torres-Peimbert S. 1981, ApJ 245, 845
Persic M., De Zotti G., Danese L., Palumbo G. G. C., Franceschini A. Boldt E. A., Marshall F. E. 1989, ApJ 344, 124
Petre R., Mushotzky R. F., Serlemitsos P. J., Jahoda K., Marshall F. E. 1993, ApJ 418, 644 (PEA93)
Pounds K. A, Nandra K., Stewart G. C., George I. M., Fabian A. C. 1990, Nature 344, 132
Raymond J. C., Smith B. W. 1977, ApJS 35, 419
Serlemitsos P. J. et al. 1995a, PASJ 47, 105
Serlemitsos P. J., Ptak A., Yaqoob T. 1995b, in The Physics of LINERS (Space Science Telescope Institute; in press) (SEA95)
Shuder, J. M., Osterbrock, D. E. 1982, ApJ 250, 55
Tanaka Y. et al. 1995, Nature 375, 659
Tanaka Y., Inoue, H., Hold S. S. 1994, PASJ 46, L37
Terashima Y., Serlemitsos P. J., Kunied, H., Iwasawa, K. 1994, in New Horizon of X-Ray Astronomy, ed F. Makino, T. Ohashi (Universal Academy Press, Tokyo) p523
Terlevich R., Melnick J. 1985, MNRAS 213, 841
Tsuru T. 1992, PhD Thesis, University of Tokyo (Physics Department)
Tsuru T. et al. 1994, in New Horizon of X-Ray Astronomy, ed F. Makino, T. Ohashi (Universal Academy Press, Tokyo) p529
Tsusaka Y. et al. 1995, Applied Optics 34, 4848
Turner T. J., Pounds K. A. 1989, MNRAS 240, 833
Ueno S., Mushotzky R. F., Koyama K., Iwasawa K., Awaki H., Hayashi I. 1994, PASJ 46, L71
Wandel A., Mushotzky R. F. 1986, ApJ 306, L61

Table 1. Log of ASCA observations of M81.

ID	Date		SIS				GIS	
	Start*	End*	Exposure†	Mode‡	X5 on§	Split♯	Exposure†	SP⋆
1	93/04/05 07:45	04/06 01:04	—	4CCD BRT	C0/C2	20	(36,039)	OF
2	93/04/07 00:55	04/08 00:53	—	4CCD BRT	C0/C2	20	(34,421)	OF
3	93/04/16 22:30	04/17 17:30	25,537	4CCD F/B	C0/C2	40	99,676	OF
4	93/04/25 14:10	04/25 21:31	10,577	4CCD F/B	C0/C2	40	14,214	OF
5	93/05/01 22:16	05/02 14:11	10,550	4CCD F/B	C0/C2	40	27,122	OF
6	93/05/18 20:47	05/19 20:30	23,530	2CCD F/B	C0/C2	40	42,864	OF
7	93/10/24 16:00	10/25 14:20	24,250	4CCD F/B	C3/C1	40	43,330	ON
8	94/04/01 05:08	04/02 03:21	28,250	1CCD FNT	C0/C2	40	41,515	ON
9	94/10/21 04:15	10/22 08:05	37,423	1CCD FNT	C2/C0	40	51,799	ON
10	95/04/01 18:50	04/02 23:10	14,813	1CCD FNT	C0/C2	40	22,625	ON

∗ The start time of observation in year/month/day hour:minutes, and the end time in month/day hour:minutes.

† Exposure time in seconds after the standard data screening described in text (subsection 3.1).

‡ The SIS mode. BRT= bright mode only, F/B = faint mode for high-bit-rate and bright mode for medium-bit rate, and FNT = faint mode only.

§ The chips of the SIS0/SIS1 detectors on which the M81 nucleus was placed.

♯ Pulse height channel for the SIS split threshold.

⋆ The GIS spread discriminator flag status.

Table 2. Model fits to the 2-10 keV spectrum of the M81 nucleus.

	SIS		GIS	
Model*	χ^2/d.o.f.	Parameter†	χ^2/d.o.f.	Parameter†
Bremsstrahlung	252/70	kT=8.8 keV	290/82	kT=8.6 keV
Power-Law	136/70	Γ=1.79 (1.76–1.81)	130/82	Γ=1.83 (1.81–1.84)
Power-Law + Gaussian‡	103/67	Γ=1.82 (1.79–1.85)	78/79	Γ=1.86 (1.84–1.88)

∗ Absorption is fixed to the Galactic line-of-sight value ($N_{\rm H} = 4 \times 10^{20}$ cm^{-2}).

† Γ is photon index, whose 90 % confidence ranges are shown in parentheses.

‡ See figure 5 for the best fit values.

Table 3. Model fits to the spectrum of the M81 nucleus in the full energy range.*

	SIS (in 0.5–10 keV)	GIS (in 0.7–10 keV)
Model 1 : Absorbed Power-Law + Gaussian†		
Photon Index	1.87 (1.85–1.89)	1.82 (1.81–1.84)
$N_{\rm H}$ (10^{20} cm^{-2}) §	9.2 (8.5–9.8)	4.7 (3.4–6.0)
χ^2/d.o.f.	133/95	122/96
Model 2: Raymond-Smith‡ + Absorbed Power-Law + Gaussian†		
kT (keV)	0.86 (0.70–1.10)	0.71 (0.63–0.80)
$L_{0.5-3}^{\rm R\text{-}S}$ (10^{38} erg s^{-1}) ♯	3.1 (1.2–6.3)	19 (13–28)
Photon Index	1.85 (1.83–1.87)	1.87 (1.85–1.90)
$N_{\rm H}$ (10^{20} cm^{-2}) §	9.4 (8.8–10.1)	17.3 (12.9–22.4)
$L_{2-10}^{P\text{-}L}$ (10^{40} erg s^{-1}) ♯	2.40 (2.37–2.43)	2.32 (2.30–2.34)
χ^2/d.o.f.	123/93	96/94

∗ The numbers in parenthesis represent the 90 % confidence range.

† The Gaussian parameters are fixed to the values from the 2–10 keV fit.

‡ Assumed to have an abundance of 0.4 times solar, and absorbed by the line-of-sight Galactic column of $N_{\rm H} = 4 \times 10^{20}$ cm^{-2}.

§ Absorption includes the line-of-sight Galactic column of $N_{\rm H} = 4 \times 10^{20}$ cm^{-2}.

♯ $L_{0.5-3}^{\rm R\text{-}S}$ is the 0.5–3 keV luminosity of the Raymond-Smith component, while $L_{2-10}^{P\text{-}L}$ is the 2–10 keV luminosity of the (unabsorbed) power-law component.

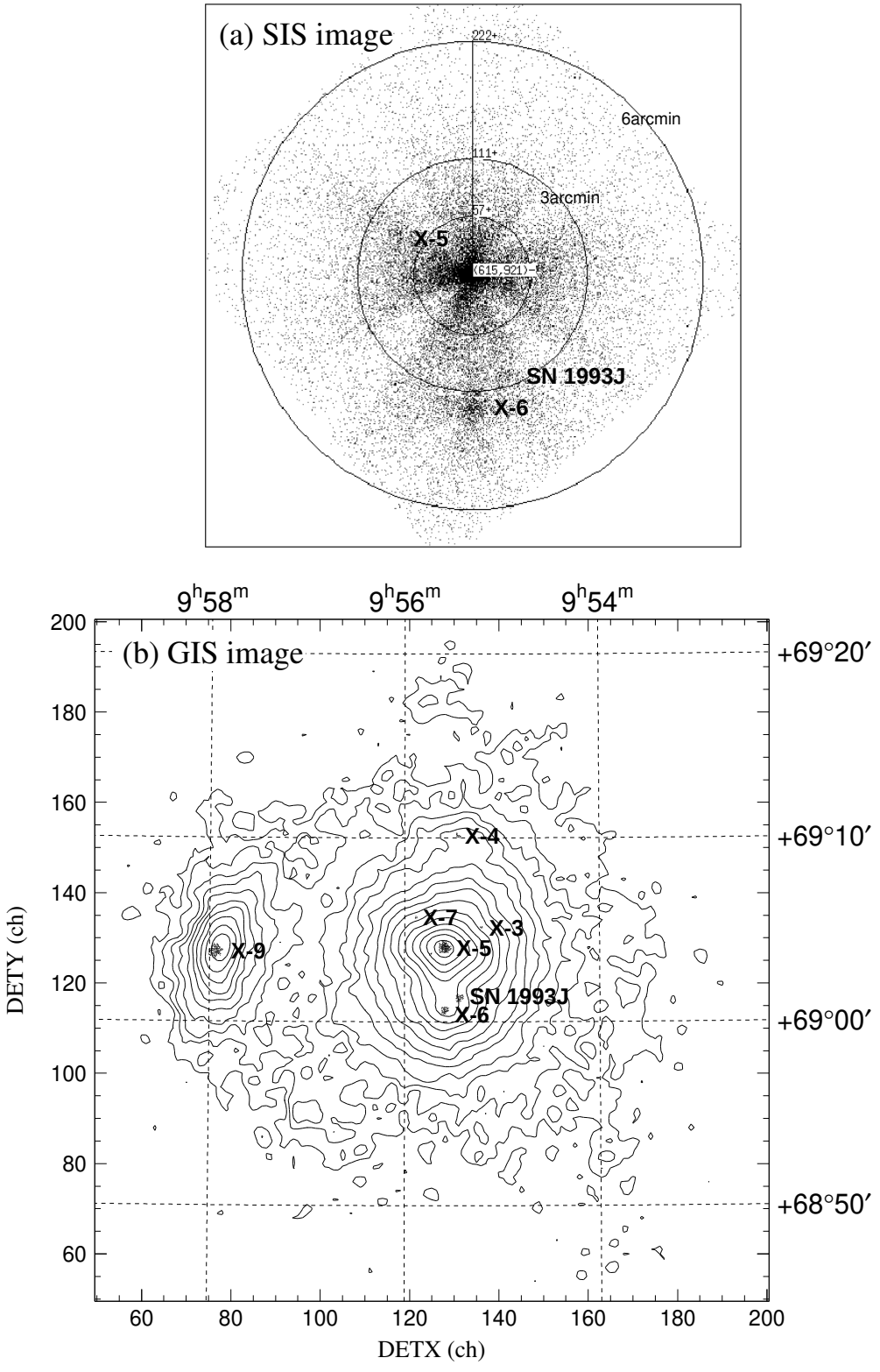

Fig. 1. X-ray images of the M81 region taken with ASCA, presented without background subtraction or vignetting correction. (a) The 0.5–10 keV SIS0 image from observation 7. SN 1993J and two Einstein sources, X-5 (the M81 nucleus) and X-6, are seen. Circles of radius 1.′5, 3′, and 6′ are drawn centered on X-5. (b) The 0.7–10 keV GIS2+GIS3 contour map smoothed with a Gaussian of σ=15″, obtained by summing data for observations 7–9. The contour levels are 2.8, 4, 5.7, 8, ... counts pixel^{-1}. An archival ROSAT HRI image taken on 1993 May, and the IPC source names, are overlaid. Sky coordinates are J2000, in which X-5 is located at ($9^{\rm h}55^{\rm m}33^{\rm s}$, $+69^\circ03'55''$).

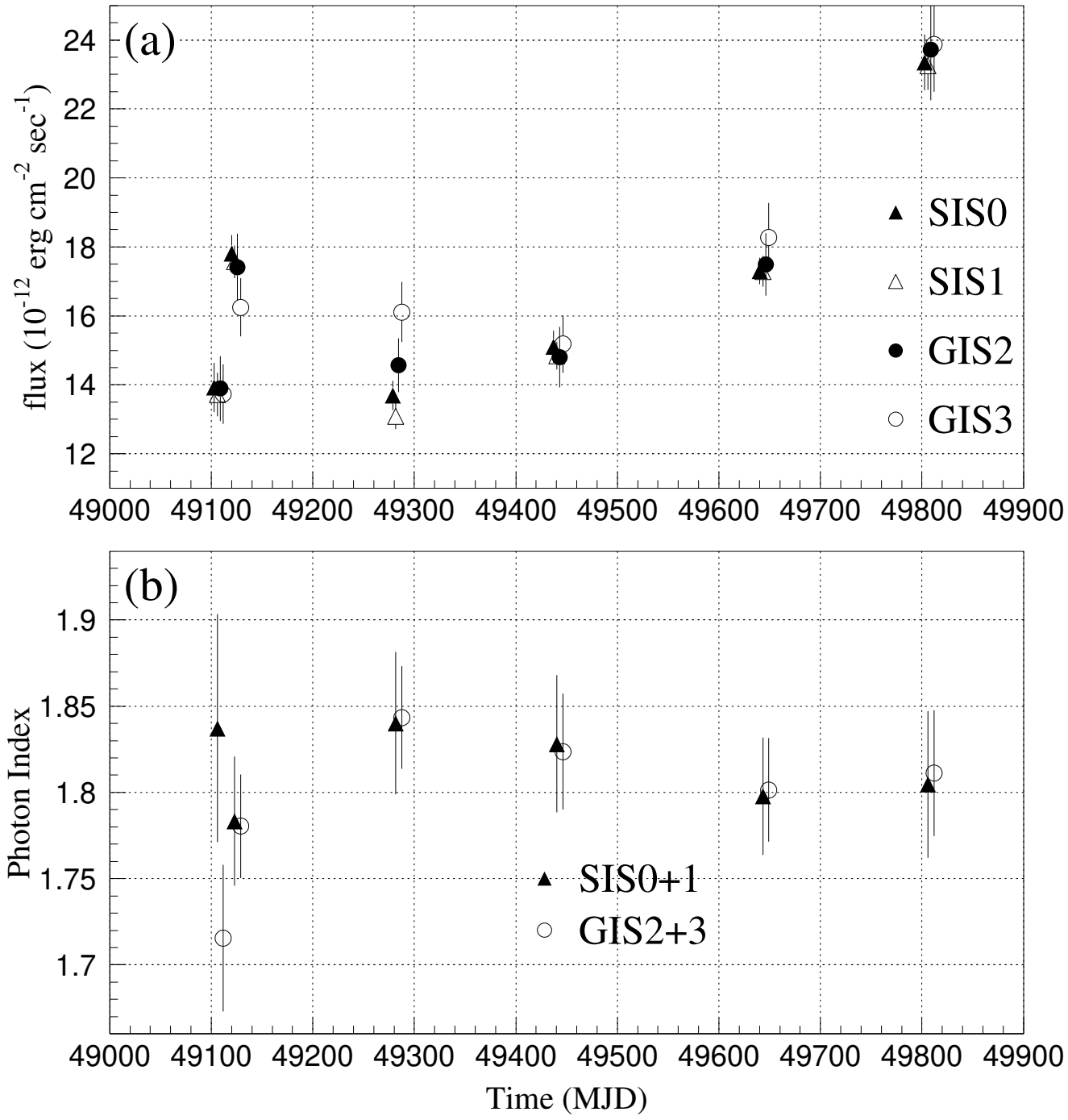

Fig. 2. Long-term 2–10 keV light curves of the M81 nucleus for observations 5 through 10, together with 90 % confidence errors. (a) The 2–10 keV flux history, obtained with SIS0+SIS1 and GIS2+GIS3. At the 3.6 Mpc distance, a flux 15×10^{-12} erg cm^{-2} s^{-1} corresponds to a luminosity 2.2×10^{40} erg s^{-1}. The observation number is given at the top. (b) History of the power-law photon index in the 2–10 keV range, determined independently with the two instruments.

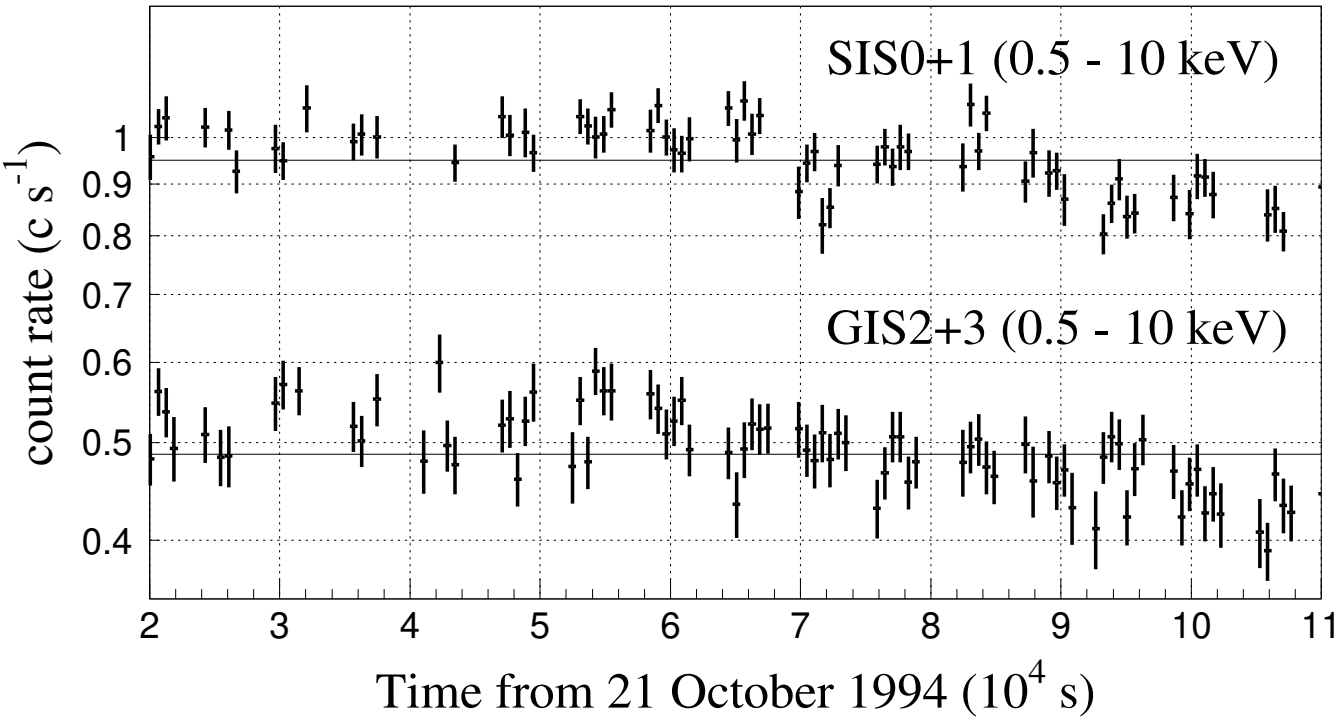

Fig. 3. Short-term 0.5–10 keV light curves of the M81 nucleus from observation 9. The upper light curve is the sum of SIS0 and SIS1, while the lower one is the sum of GIS2 and GIS3. Each bin is 600 s long, and errors are 1σ. Solid lines indicate averaged counting rates (0.95 c s^{-1} for the SIS and 0.49 c s^{-1} for the GIS).

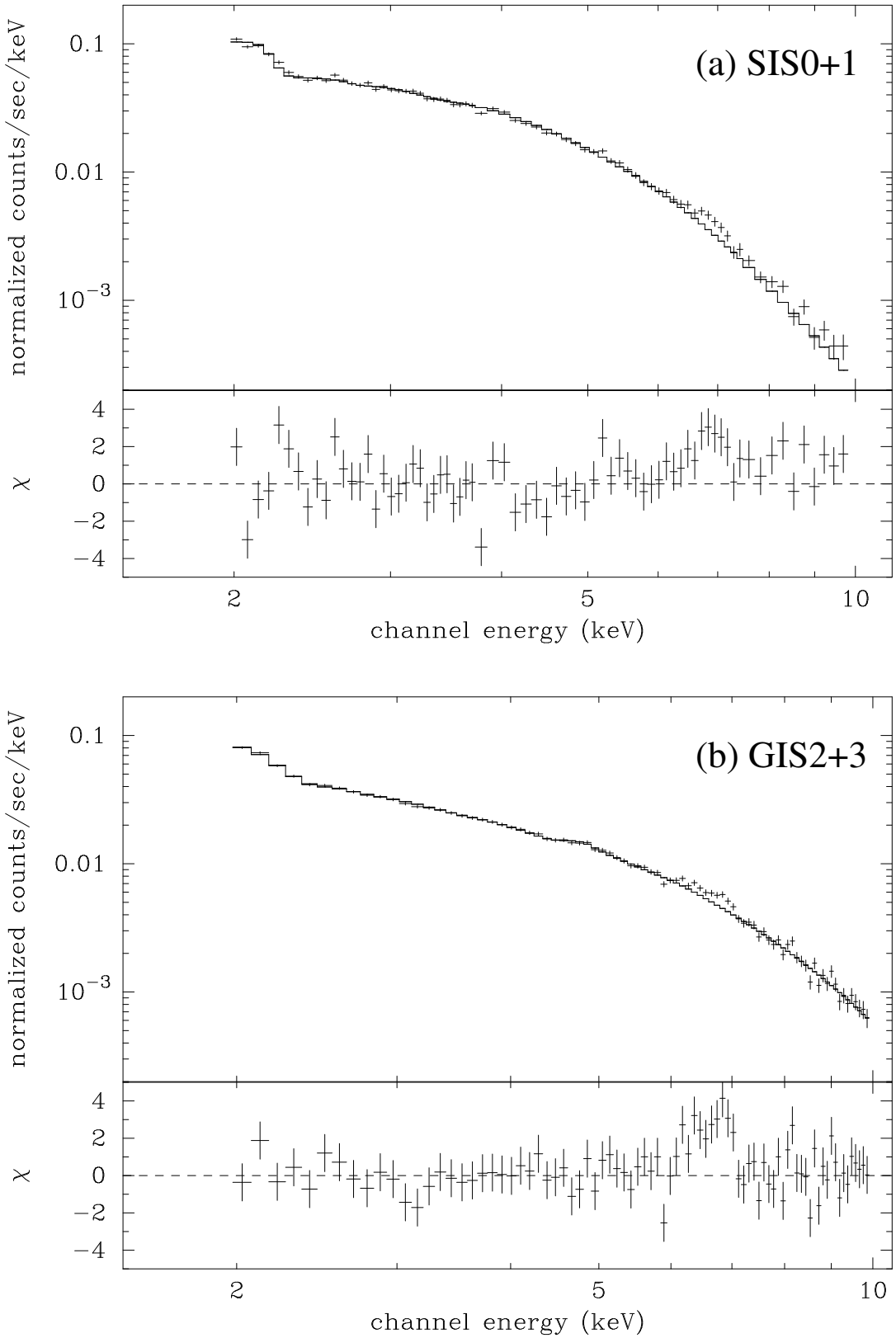

Fig. 4. The SIS (panel a) and GIS (panel b) spectra of the M81 nucleus in the 2–10 keV band, both summed over observations 3–10. The solid lines show the best-fit power-law model convolved through respective instrumental responses, and the fit residuals are shown in lower panels. The fitting ignored the 6–7.5 keV region, where the iron line feature is clearly seen.

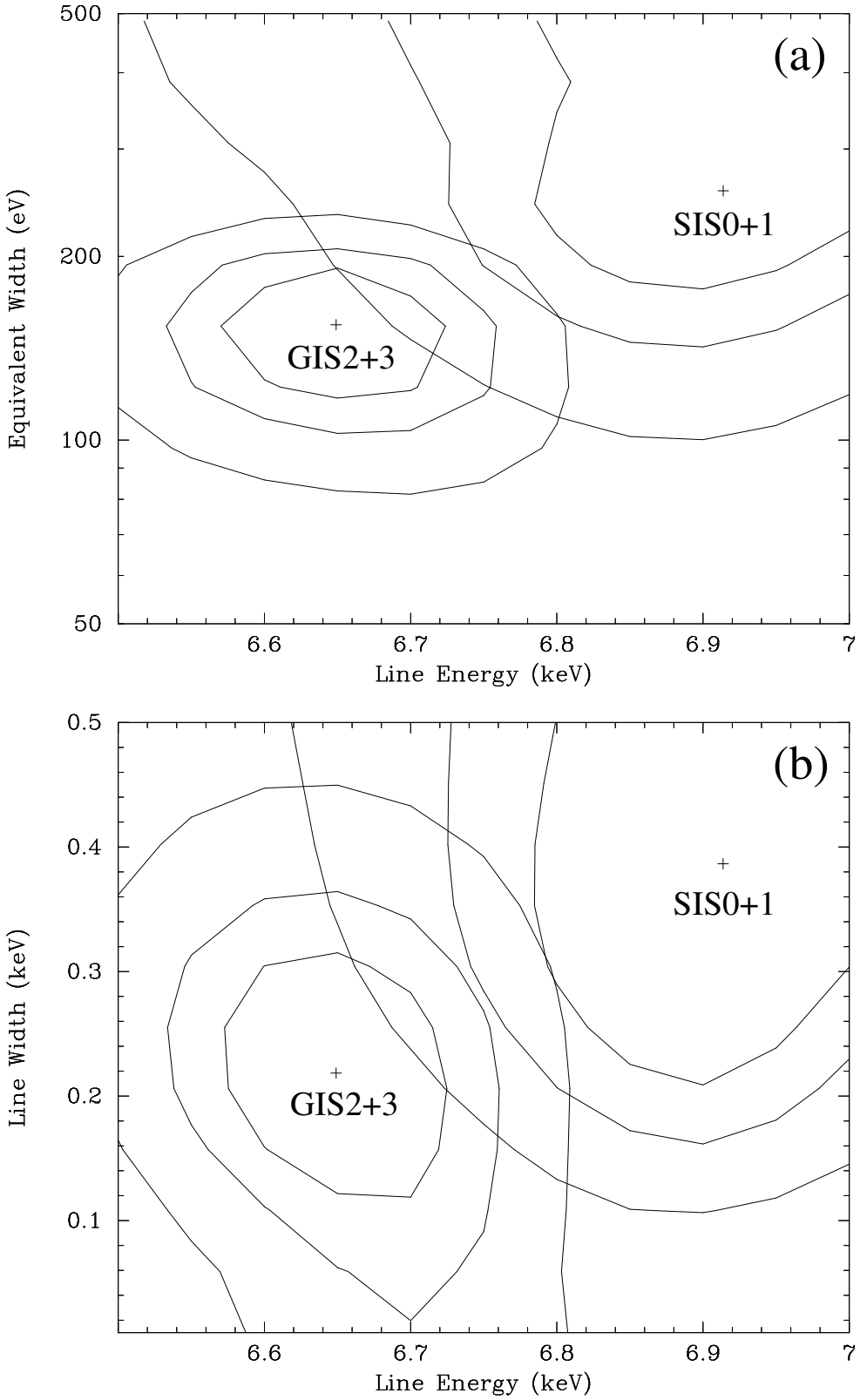

Fig. 5. Confidence contours of the iron line parameters, determined separately with the SIS and GIS by fitting a broad Gaussian model to the spectra of figure 4. Contours (from inner to outer) represent 68, 90, and 99 % confidence levels, and the cross indicates the best-fit solution. (a) Line center energy vs. line equivalent width. (b) Line center energy vs. line width (Gaussian σ).

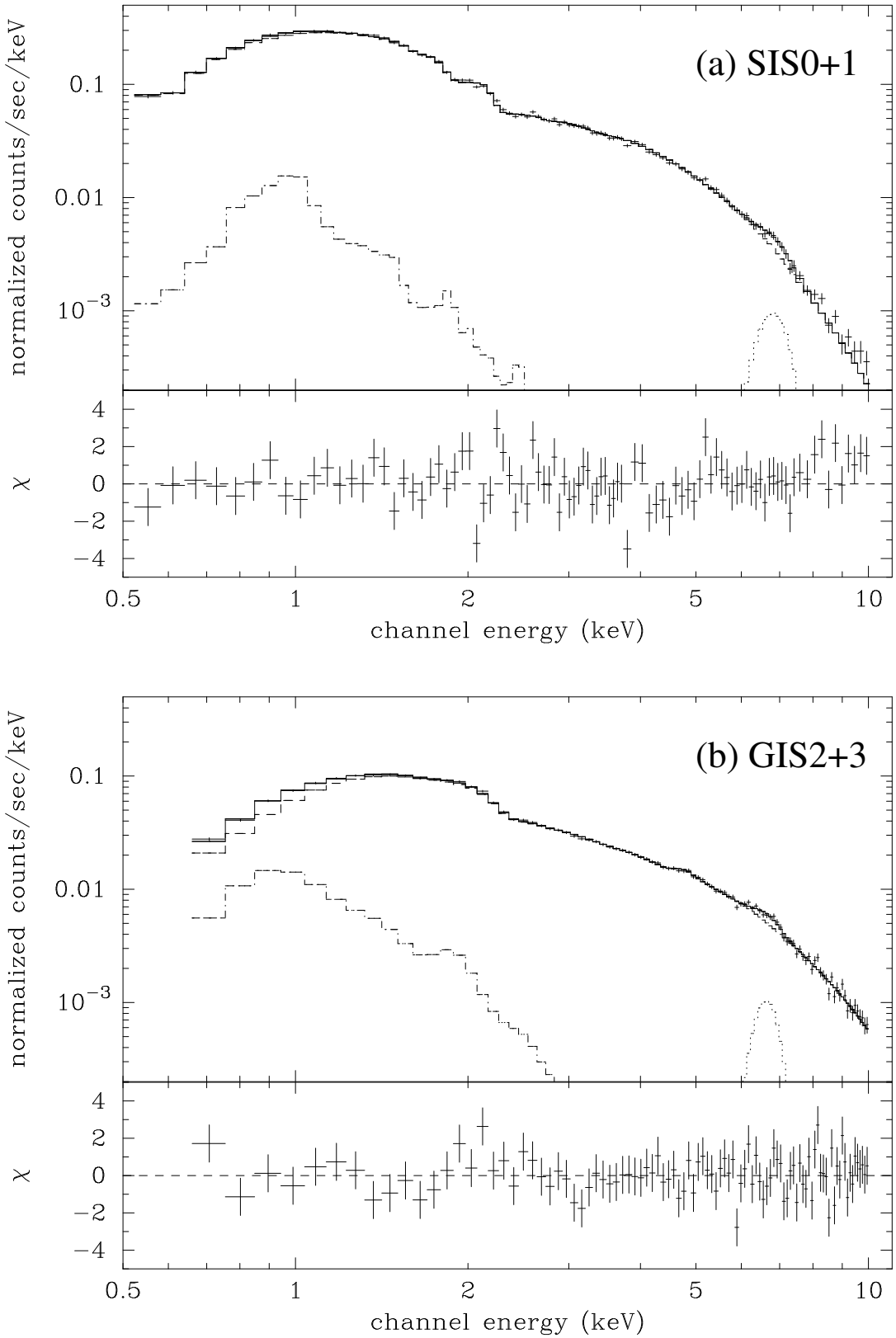

Fig. 6. The same as figure 4, but shown over the full energy bands. Solid lines indicate the best-fit solution of Model 2 in table 3, which consists of three components; a Raymond-Smith model (dot-dashed), an absorbed power-law (dashed), and a broad Gaussian (dotted). The fit is not simultaneous between the two instruments.